


# Novel Nanozyme-Based Multicomponent in situ Hydrogels with Antibacterial, Hypoxia-Relieving and Proliferative Properties for Promoting Gastrostomy Tube Tract Maturation

Feng Xiao<sup>1</sup> <sup>\*</sup>, Bisong Yan<sup>2,\*</sup>, Tianwen Yuan<sup>2</sup>, Yang He<sup>2</sup>, Xiaojun Zhang<sup>3</sup>, Xiaoyun He<sup>1</sup>, Wei Peng<sup>1</sup>, Ying Xu<sup>3</sup>, Jun Cao<sup>1,4</sup>

<sup>1</sup>Shanghai Eighth People's Hospital, Xuhui District, Shanghai, 200030, People's Republic of China; <sup>2</sup>Department of Interventional Oncology, Dahua Hospital, Xuhui District, Shanghai, 200237, People's Republic of China; <sup>3</sup>College of Pharmacy, Jiangsu University, Zhenjiang, 212013, People's Republic of China; <sup>4</sup>Shanghai University of Medicine and Health Science, Pudong New Area, Shanghai, 201318, People's Republic of China

\*These authors contributed equally to this work

Correspondence: Jun Cao, Shanghai Eighth People's Hospital, Xuhui District, Shanghai, 200030, People's Republic of China, Email juncao11@sina.com; Ying Xu, College of Pharmacy, Jiangsu University, Zhenjiang, 212013, People's Republic of China, Email ingyx@sina.com.cn

**Purpose:** Gastrostomy is the commonly used enteral feeding technology. The clinical risks caused by tube dislodgement and peristomal site infection are the common complications before complete tract maturation after gastrostomy. However, there is currently no relevant research to promote gastrostomy wound treatment and tract maturation.

**Methods:** Herein, a nanozyme loaded bioactive hydrogels (MO-HPA) was developed to accelerate tract maturation and inhibit bacteria. Nano-manganese dioxide (n-MO) and polylysine modified hyaluronic acid (HP) were synthesized and characterized. In situ hydrogels were prepared by mixing the HP/alginate solution, and the n-MO solution containing Ca<sup>2+</sup>. The structure, physicochemical and mechanical properties of MO-HPA were evaluated. Furthermore, the antibacterial activity, and the In vitro and intracellular oxygen production efficacy were determined. The cell migration, wound healing and tube tract maturation promotion effect were assessed in cell experiments and in skin defect mouse model, as well as rabbit gastrostomy model.

**Results:** The n-MO has a uniform particle size with oxygen producing activities. The MO-HPA demonstrated a homogeneous and porous microstructure. Additionally, the gelation time, swelling ratio, rheological behavior, and mechanical properties of hydrogels could be tuned by adjusting the HP content. The antibacterial efficiency of the MO-HPA<sub>1.0</sub> group on *E. coli* and *S. aureus* increased by about 40.1% and 55.6% respectively, compared to the MO-HPA<sub>0.5</sub> group. Additionally, MO-HPA<sub>1.0</sub> hydrogel demonstrated effective oxygen-producing and cell migration-promoting functions in both in vitro and cellular experiments. The MO-HPA<sub>1.0</sub> group significantly accelerated wound healing in both of mouse skin defect model and rabbit gastrostomy model. The hydrogel group exhibited a significant promotion in collagen content and reduction in HIF-1 $\alpha$ , which effectively hastened tract maturation.

**Conclusion:** Therefore, our study provides new and critical insights into a strategy to design bioactive hydrogels with multiple functions, which can open up a new avenue for accelerated wound healing after gastrostomy.

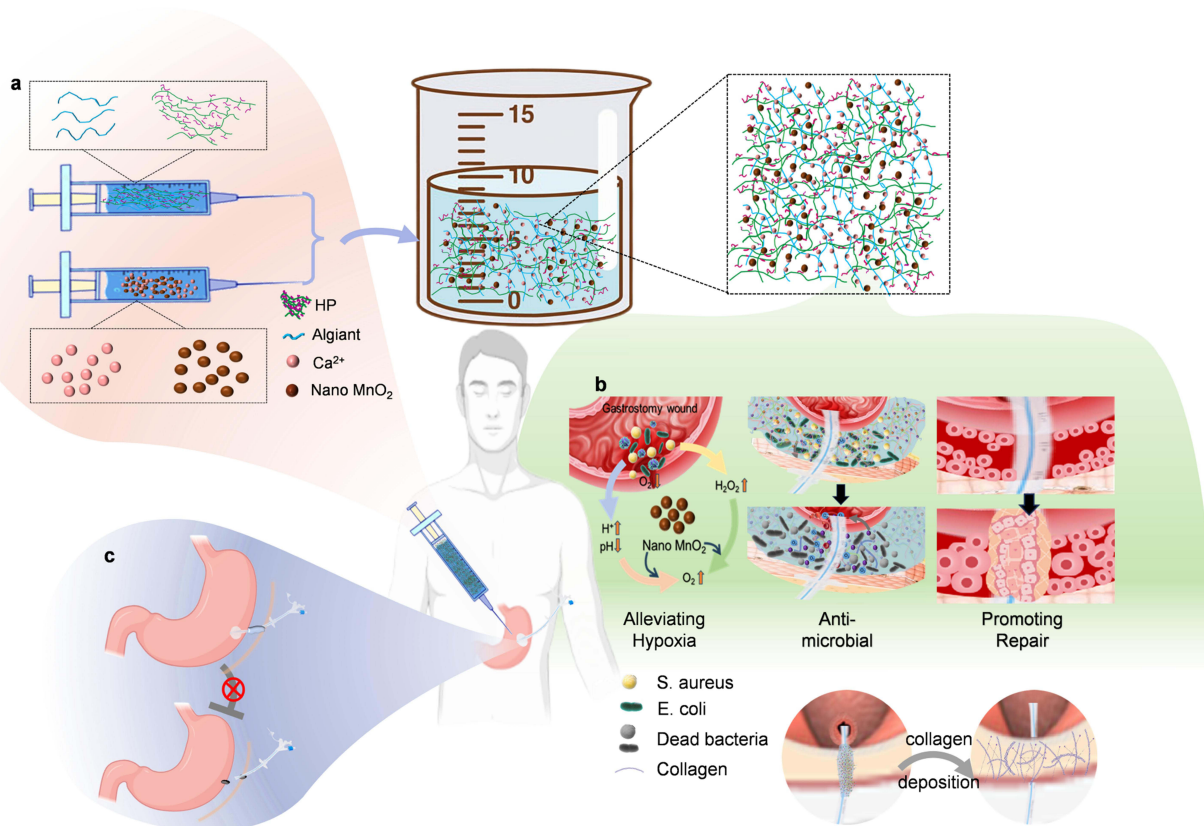
**Keywords:** gastrostomy, nano-manganese dioxide, multifunctional hydrogels, antibacterial, accelerated treatment

## Introduction

Enteral feeding is the preferred method for the mid- to long-term enteral feeding of patients with a functional gastrointestinal system but difficulty swallowing. Enteral administration has the advantages of maintaining the intestinal microbiota balance and reducing the risk of bacterial translocation and associated bacteremia.<sup>1</sup> Gastrostomy is the most commonly used enteral feeding technology and has been used with neurological diseases, such as cerebrovascular disease, retardation and dementia, and head and neck cancer.<sup>2</sup> International guidelines recommend gastrostomy for



## Graphical Abstract



patients who require enteral access for more than 4 to 6 weeks,<sup>3</sup> as gastrostomy is considered a safe technique.<sup>4</sup> However, some complications, including bleeding, tube dislodgement, peristomal site infection, and peristomal leakage, have been reported, which bring great pain and danger to the patient.

Among these complications, gastrostomy tube dislodgement and peristomal site infection deserve more attention. Peristomal site infection is the most common complication following gastrostomy, with a rate of incidence ranging from 4% to 30%,<sup>5</sup> even reaching 65% as reported in some studies.<sup>6</sup> Nevertheless, deep tissue infections are difficult to detect in the early stages. Currently, the main approach to treat peristomal site infection is to periodically administer antibiotics to reduce the incidence of infection.<sup>7</sup> Inadvertent tube dislodgement is also a common complication, with an incidence rate of approximately 4%-13%.<sup>8</sup> It is estimated that gastrostomy tract formation occurs within the first 2 weeks after gastrostomy, but complete tract maturation may be delayed for up to 1 month after the procedure.<sup>2</sup> If tube displacement occurs in the immature tract, the stomach and anterior abdominal wall separate, resulting in clinical risks, such as free perforation, misplacement of the reset blind tube into the peritoneal cavity and leakage into the peritoneal cavity.<sup>9</sup> However, replacement of the tube can be performed blindly at the bedside after the tract is mature. Thus, accelerating tract maturation is an effective way to reduce the clinical risks caused by tube displacement. Currently in clinical practice, traditional dressings for post-gastrostomy wounds, such as split gauze, require daily replacement and are ineffective in preventing infections, therefore, with postoperative wound infection rates reaching as high as 47.05%.<sup>10,11</sup> Hydrogel dressings can increase wound moisture, but their mechanical properties and lack of antimicrobial action are limiting factors. Incorporating antimicrobial drugs into wound dressings is a common method, but excessive use of antibiotics can lead to antibiotic resistance, reducing their effectiveness in treating infections.<sup>12,13</sup> Until now, there

was little research on promoting tract maturation or preventing infection with nonantibiotic drugs after gastrostomy. Thus, exploring the development of new dressing coatings on tubes that can prevent infection and accelerate tract maturation is of great significance for reducing the complications of gastrostomy.

Oxygen is an important factor in wound treatment. During the healing process, processes such as collagen synthesis and cell proliferation need sufficient oxygen to provide energy.<sup>14,15</sup> It has been reported that collagen synthesis requires an oxygen tension of approximately 30–40 mmHg, while cell proliferation can vary depending on the cell type but generally requires similar levels.<sup>16</sup> However, local wound hypoxia due to poor oxygen diffusion and permeation caused by damaged blood vessels and tissue tightness is a major reason for poor wound healing.<sup>17,18</sup> Additionally, bacterial colonization is inevitable in chronic wounds, which attracts leukocytes, leading to elevated levels of pro-inflammatory cytokines. Consequently, this directly triggers and sustains the inflammatory response, and therefore resulting in an elevated level of reactive oxygen species (ROS), such as  $H_2O_2$  and superoxide ( $O_2^{\cdot-}$ ), which is detrimental to wound healing.<sup>14,19</sup> Excessive ROS can lead to the over-cross-linking of collagen, resulting in a stiff and non-functional extracellular matrix. Moreover, the oxidative stress triggered by excessive ROS not only impedes cell migration but also impair angiogenesis by damaging endothelial cells and disrupting the vascular network.<sup>20,21</sup> Some methods to topically apply oxygen to tissue have been proposed, such as using hyperbaric dissolved oxygen or perfluorodecalin.<sup>22</sup> However, these techniques can only improve the oxygen level of the wound but cannot regulate the excessive level of ROS. Nanozymes, such as iron oxide, manganese oxide, and cerium oxide, are a type of nanometal oxide that has received widespread attention in recent years. Nanozymes can catalyze the reduction of  $H_2O_2$  to generate oxygen to scavenge ROS and supply oxygen. Among them, nano-manganese dioxide (n-MO), which possesses good safety and a strong catalytic ability in acidic environments, is suitable for application in gastric acid environments after gastrostomy.

Due to their excellent biocompatibility and flexibility, hydrogels are widely used in wound healing.<sup>23</sup> Hyaluronic acid (HA), a disaccharide glycosaminoglycan composed of D-glucuronic acid and N-acetylglucosamine,<sup>24</sup> is a natural component of the extracellular matrix (ECM), connective tissue, epithelial tissue, and nerve tissue.<sup>25</sup> As an important component of the ECM, HA is widely used in tissue engineering and wound treatment research and exhibits the potential to promote cell migration.<sup>26,27</sup> Polylysine (PLL) is a synthetic peptide produced by polymerizing lysine monomers that has good safety and biocompatibility.<sup>28</sup> PLL has good cell membrane affinity due to its positive charge and has thus been used for improving cell adhesion in damaged blood vessels.<sup>29</sup> Moreover, PLL possesses broad-spectrum antibacterial activities against both gram-negative and gram-positive bacteria.<sup>30</sup> Additionally, PLL has low drug resistance due to its ability to interact with microbial membranes.<sup>31</sup> Sodium alginate has unique properties, such as being nontoxic, biodegradable, biostable, and viscousifying, which have led to it being widely used as a wound dressing material.<sup>32</sup> In the presence of cations such as  $Ca^{2+}$ , sodium alginate crosslinks to form a hydrogel with a three-dimensional network. Alginate hydrogels (AL) can provide a moist microenvironment, absorb wound exudate, and promote cell proliferation, which facilitate wound healing.<sup>33,34</sup> Considering that hydrogels prepared by monomers are limited by due to having few functions,<sup>35,36</sup> composite materials have been developed to fabricate multifunctional hydrogels.<sup>37</sup> However, the problems of insufficient mechanical strength and inconvenient use still exist in some composite hydrogels. In situ hydrogels, with the advantages of being convenient and suitable for wounds of different sizes and shapes, have been widely studied for use in wound dressings. Therefore, we designed a novel ternary in situ hydrogel composed of HA, PLL and alginate with ideal mechanical properties, adhesion characteristics and antibacterial activity to promote tract maturation and prevent infection after gastrostomy.

Considering the above, n-MO-doped multifunctional in situ hydrogels (MO-HPA hydrogels) were developed to have antibacterial, ROS scavenging and hypoxia relief activities to promote tract maturation and reduce complications after gastrostomy. To the best of our knowledge, this is the first time to use multifunctional hydrogels in preventing gastrostomy infection and promoting tract maturation. Compared to existing wound dressing solutions, such as silver-impregnated dressings, alginate dressings, and hydrocolloids, which often suffer from limitations such as insufficient antibacterial efficacy, lack of oxygen-generating capacity, and suboptimal mechanical strength, our MO-HPA hydrogels offer a significant advancement. PLL modified HA (HP), with cell migration and antibacterial properties was synthesized. Then, n-MO-doped in situ ternary hydrogels crosslinked by HP and alginate with good mechanical properties and adhesion properties were developed. The physical and chemical properties of the hydrogels, such as morphology,

rheology, gel formation, and mechanical properties, were evaluated *in vitro*. The ROS scavenging and O<sub>2</sub> supplying functions of the MO-HPA hydrogels were confirmed by *in vitro* and cell assays, and their abilities to resist bacteria and promote cell migration were detected *in vitro*. Finally, the effects of the *in situ* hydrogel on healing acceleration and the promotion of tract maturation were evaluated in a mouse wound model and rabbit gastrostomy model, respectively.

## Materials and Methods

### Materials

Hyaluronic acid (HA, Mw = 1200 kDa) was obtained from Shandong Haiyu Forida Co., Ltd. (Shandong, China). Sodium alginate (SA, MW = 480 kDa, M/G ≈ 1) was purchased from Shanghai Macklin Biochemical Co., Ltd. (Shanghai, China). Epsilon-polylysine (Mw = 4 kDa) was procured from Zhengzhou Qihuateng Co., Ltd. (Zhengzhou, China). 1-(3-Dimethylaminopropyl)-3-ethylcarbodiimide hydro (EDC), N-hydroxysuccinimide (NHS) and Bovine serum albumin (BSA) were obtained from Sigma-Aldrich (St. Louis, Missouri, USA). Potassium permanganate (KMnO<sub>4</sub>) was received from Sinopharm Co., Ltd. (Shanghai, China). Tris(4,7-biphenyl-1,10-o-phenanthroline) ruthenium dichloride (RDPP) (98%) was procured from Leyuan Biological Co., Ltd. (Hangzhou, China).

### Synthesis and Characterization of Nano-MnO<sub>2</sub>

Nano-MnO<sub>2</sub> (n-MO) was prepared by the redox method with some modifications (Wang, Song, Zhu, Zhang, and Liu, 2018). Briefly, KMnO<sub>4</sub> solution (7 mg/mL) was added dropwise to BSA solution (15 mg/mL) and stirred at room temperature. Next, the mixed solution was dialyzed (MWCO 8–14 kDa) against deionized water (DI water). Finally, the product (n-MO) was obtained by lyophilization and stored at 4 °C. The ultraviolet absorption spectra of KMnO<sub>4</sub>, BSA and n-MO were acquired with an ultraviolet spectrophotometer (UV-1800PC, MAPADA, Shanghai, China). The morphology of n-MO was examined using transmission electron microscopy (TEM, JEOL 2100 PLUS, Tokyo, Japan). The particle size and zeta potential were determined by dynamic light scattering (DLS, 90Plus PALS, Brookhaven, New York, USA). The ability of n-MO to catalyze H<sub>2</sub>O<sub>2</sub> to produce oxygen was determined by Tris (4,7-biphenyl-1,10-o-phenanthroline) ruthenium (II) dichloride (RDPP). Briefly, a certain amount of RDPP (3 mM) ethanol solution was added to PBS (pH 4.0 or pH 7.4) without or with different concentrations of H<sub>2</sub>O<sub>2</sub>. After the addition of n-MO, the fluorescence spectra of the samples were acquired by using a fluorescence spectrophotometer (F97XP, Lengguang Technology, Shanghai, China) with an excitation wavelength of 455 nm and emission wavelength of 615 nm.

### Synthesis and Characterization of PLL Modified HA

PLL modified HA (HP) was synthesized as described in a previous study with some modifications. In brief, 1.2 g of HA was dissolved in 60 mL of PBS (pH 5.5) to obtain a HA solution. Then, 19.1 mg of EDC and 21.7 mg of NHS were dissolved in DI water (40 mL) and added to the HA solution under stirring. The reaction continued for 1 h at 4 °C. Afterward, different proportions of PLL (13.3 mg, 26.6 mg, or 66.7 mg) were added to the reaction solution. After adjusting the pH to 7, the reaction proceeded for another 4 h under room temperature. Subsequently, the solution was dialyzed against water for 48 h and then lyophilized to obtain HP with different ratios of the starting materials (referred to as HP<sub>10</sub>, HP<sub>20</sub> and HP<sub>50</sub>).

The modified HP materials with different ratios of starting materials were qualitatively confirmed by attenuated total reflection infrared spectroscopy (ATR, Thermo Scientific™ Nicolet™ iS50, Shanghai, China). The chemical composition of the optimized HP was analyzed with a <sup>1</sup>H nuclear magnetic resonance (<sup>1</sup>H NMR, AVANCE II 400 MHz, Switzerland) spectrometer.

### Preparation of the Multifunctional MO-HPA Hydrogels

n-MO-doped multicomponent *in situ* hydrogels (composed of HP and alginate, MO-HPA) were prepared using the following procedures. Appropriate amounts of SA and HP were dissolved in water to obtain solution A. n-MO was dispersed in CaCl<sub>2</sub> solution (1.5%) to obtain solution B. The *in situ* hydrogels were prepared by mixing solution A and solution B at a ratio of 5:1. The hydrogels were named MO-HPA<sub>0.5</sub>, MO-HPA<sub>1.0</sub> and MO-HPA<sub>1.5</sub> according to the HP<sub>20</sub>

concentration in solution A (0.5%, 1.0% and 1.5%, respectively). HPA hydrogels without n-MO were prepared by the same procedure, except that solution B contained only CaCl<sub>2</sub>.

## Characterization of MO-HPA Hydrogels

The internal morphology of the MO-HPA hydrogels was observed by scanning electron microscopy (SEM, JSM 7001F, Japan) after lyophilization. The gelation times of the hydrogels were measured by the vial tilting method. Briefly, solutions A and B were injected into the vial simultaneously at room temperature, and the time at which the hydrogel formed and stopped flowing was recorded.

The swelling behaviors of hydrogels were also evaluated.<sup>38</sup> MO-HPA hydrogels (about 3 mg) was weighed ( $W_0$ ) before immersion in 10 mL of PBS (pH 7.4) at 37 °C. The hydrogels were removed from the PBS solution at specified time intervals and weighed after removing the water on the surface of the hydrogels ( $W_1$ ). The swelling ratio was calculated using the following formula (1).

$$\text{swelling ratio} = \frac{(W_1 - W_0)}{W_0} \times 100\% \quad (1)$$

## Injectability and Self-Healing Properties

Solution A was stained with bromophenol blue and injected into solution B using a 23G needle to investigate the injectability and formability. Smooth letters “DH” and “UJS” were written by injection, and the letter “J” was lifted to evaluate the self-healing ability. Hydrogel blocks stained or not with bromophenol blue were cut into separated pieces. Subsequently, the cut interfaces were joined without external intervention to heal, and the self-healing behaviors of the hydrogels were observed with a digital camera and images were acquired at the predetermined time under. These studies were conducted under room temperature.

## Cytocompatibility, Cell Migration Capability

The cytocompatibility of the hydrogels was assessed by using the MTT method. 3T6-Swiss albino cells were purchased from Procell Life Science & Technology Co., Ltd, Wuhan. Briefly, 3T6-Swiss albino fibroblasts cells (mouse fibroblasts) were seeded in 96-well plates ( $1 \times 10^4$  cells/well) and cultured in high-glucose Dulbecco's modified Eagle's medium (DMEM) containing 10% bovine fetal serum for 24 h at 37 °C with 5% CO<sub>2</sub> and 95% relative humidity. Afterward, the culture medium was replaced with DMEM containing a series of concentrations of sterilized n-MO, MO-HPA<sub>0.5</sub>, MO-HPA<sub>1.0</sub> or MO-HPA<sub>1.5</sub>. After culturing for 24, 48 or 72 h, the culture medium was discarded, and the cells were washed with PBS. Cell activity was detected by using MTT solution, and the absorbance at 570 nm was recorded by a microplate reader (BioTek 800 TS, Vermont, USA) to calculate cell viability.

To investigate the cell migration capability bestowed by treatment with the MO-HPA hydrogels, cell scratch tests were performed. Specifically, 3T6 cells were inoculated in 6-well plates ( $1 \times 10^6$  cells/well) and cultured for 24 h. Afterward, the cell surface was scratched vertically with a 200  $\mu$ L pipetting tip and washed with DMEM. Next, the cells were treated with DMEM as control group, while experimental groups were treated with DMEM medium containing different concentrations of hydrogels (MO-HPA<sub>0.5</sub>, MO-HPA<sub>1.0</sub>, or MO-HPA<sub>1.5</sub>) for 24 hours. Then, the scratched area of the cells was photographed by using an inverted fluorescence microscope (Nikon TI-DH, Tokyo, Japan) to evaluate wound healing efficacy.

## In vitro and Intracellular Oxygen Production Efficacy of MO-HPA

The in vitro oxygen production efficacy of the hydrogels with or without n-MO (MO-HPA or HPA) under different pH conditions was examined by using the fluorescent probe (RDPP). In brief, RDPP ethanol solution (3 mM) was diluted by PBS (pH 7.4, 4.0 or 1.5) without or with H<sub>2</sub>O<sub>2</sub>. After the addition of MO-HPA<sub>1.0</sub> or HPA<sub>1.0</sub> hydrogels, the fluorescence spectra of the samples were acquired by using a fluorescence spectrophotometer (F97XP, Lengguang Technology, Shanghai, China) with an excitation wavelength of 455 nm and emission wavelength of 615 nm at set times.

NIH-3T6 cells were inoculated in 6-well plates ( $1 \times 10^5$  cells/well) under hypoxic conditions for 24 h. Then, the cells were treated with 5  $\mu$ M RDPP (diluted in blank DMEM) for 4 h. After washing with PBS, the cells were incubated with HPA<sub>1.0</sub> or MO-HPA<sub>1.0</sub> for 24 h. Finally, the cells were observed by an inverted fluorescence microscope (ECLIPSE Ti, Nikon, Tokyo, Japan).

## Antibacterial Properties

The antibacterial properties of the MO-HPA hydrogels were evaluated by using *Escherichia coli* (*E. coli*, gram-negative bacterium) and *Staphylococcus aureus* (*S. aureus*, gram-positive bacterium). The inhibition of *E. coli* by the hydrogels was determined by the spread plate method. In brief, equal proportions of hydrogels with different concentrations were added to activated *E. coli* solution. Subsequently, the *E. coli* was coated in the medium at a concentration of  $10^8$  CFU/mL. After culturing in a constant temperature (37 °C) shaker for 24 h, the inhibition performance of the hydrogel was determined by observing and counting the number of *E. coli* bacterial colonies. The antibacterial properties of MO-HPA against *S. aureus* were detected following a similar method.

## Rheology, Mechanical Properties, and Adhesion Ability

The rheological properties of the hydrogels (MO-HPA<sub>0.5</sub>, MO-HPA<sub>1.0</sub> and MO-HPA<sub>1.5</sub>), such as the time sweep, strain sweep, oscillatory frequency sweep and coefficient of shear viscosity, were evaluated by a rheometer (DHR-2, TA-Instruments, Massachusetts, USA). The mechanical properties of the MO-HPA hydrogels were measured by a universal material testing machine (MTS, CMT2103, Minnesota, USA). The compression capabilities of the hydrogels cut into cylinders (10 mm  $\times$  5 mm) were tested at a speed of 20 mm/min at 100 N. The adhesion properties of the MO-HPA hydrogels were quantitatively evaluated by a lap shear test. Briefly, hydrogel layers (10 mm  $\times$  10 mm) were adhered between the surface of two fresh porcine skins (30 mm  $\times$  30 mm). Subsequently, MTS was used to perform the tensile test with a 50 N force measuring element at a speed of 10 mm/min at room temperature.

## Hemolysis Assay

Rabbit blood was collected in a heparinized tube. After centrifugation, the cell precipitates were collected and washed several times with PBS (pH 7.4) and then dispersed in PBS to obtain an erythrocyte dispersion. Solutions of MO-HPA<sub>1.0</sub> at different concentrations (0.5, 1.0, 2.5, 5.0, 10, 20 mg/mL) were dispersed into 0.5 mL of the erythrocyte dispersion as the experimental groups. DI water and PBS were used as positive and negative controls, respectively. Each group was incubated at 37 °C for 2 h, and the cell morphology was observed under a microscope.

## In vivo Study

### Animals

Balb/c mice (male, 6–8 weeks, 20–30 g) and rabbits (male, 5–6 months, 1.5–2.5 kg) were provided by Jiangsu University Animal Center (Zhenjiang, China). All animal protocols in this study were approved by the Institutional Animal Care and Use Committee of Jiangsu University (UJS-IACUC-2022091302), and met the guidelines of the National Research Council's Guide for the Care and Use of Laboratory Animals.

## Wound Healing of Full-Thickness Skin Defects in Mice

To evaluate the effect of MO-HPA<sub>1.0</sub> on wound healing, a full-thickness skin defect model was established.<sup>39</sup> In brief, after anesthesia, a circle of about 0.5 cm  $\times$  0.5 cm was marked on the mid-back of Balb/c mice and excised with surgical scissors to create a full-thickness skin defect wound. Then, all the mice were randomly divided into two groups. One group of mice were treated with the hydrogels (MO-HPA<sub>1.0</sub>) once a day, and the other group was treated with normal saline as control group. Wound healing was observed at preset time points. The wound closure was evaluated by Image J. The wound area measured at day 0 was recorded as  $S_0$ , while its wound area measured at days 1, 3, 5, 7, and 14 was recorded as  $S_t$ , and the wound healing ratio was calculated by following formula (2).

$$\text{wound area} = \frac{S_t}{S_0} \times 100\% \quad (2)$$

## Acceleration of Tract Maturation in a Rabbit Gastrostomy Model

The effect of MO-HPA<sub>1.0</sub> to enhance tract maturation was evaluated in a rabbit gastrostomy model. Due to the inconvenience of endoscopic technology in animal laboratories, a surgical and suturing method was conducted to establish a rabbit gastrostomy model. In brief, the rabbits were randomly divided into two groups. A small opening was created in the rabbit abdominal cavity near the upper edge of the stomach, and then a very small hole was cut in the stomach. Afterward, a thin tube with a ball head was carefully inserted into the stomach of the rabbit through the abdominal wall. In the control group, the tube was left untreated, whereas the tube of treatment group was coated with MO-HPA<sub>1.0</sub>. The skin around the incision was then carefully sutured. The rabbits were sacrificed on days 0, 7, and 14 after gastrostomy, and the maturity of the tract was determined anatomically.

## Histological Examination and Immunohistochemical Analysis

For histological analysis, rabbits were sacrificed on days 0, 5, and 14. The stomach wound samples around the tube were retrieved and fixed in 10% formalin for histological analysis, Masson staining and immunohistochemistry (HIF-1 $\alpha$ ). The collagen volume fraction and HIF-1 $\alpha$  positive density of wound tissues were analyzed and calculated using ImageJ software. In addition, the gastric tissue homogenates on days 7 and 14 were centrifuged, the inflammatory factors (TNF- $\alpha$ , IL-1 $\beta$ , and IL-6) were determined by ELISA kit.

## Statistics

The experimental data are expressed as the mean  $\pm$  standard deviation. Statistical analyses were performed by one-way ANOVA followed by Tukey's multiple comparison tests. A value of *p* less than 0.05 was considered to indicate statistical significance.

## Results and Discussion

### Synthesis and Characterization of Nano-MnO<sub>2</sub>

In the modified redox synthetic method, BSA served as both the biological template and reductant. As shown in [Figure 1a](#), n-MO had an average hydrodynamic diameter of approximately 40 nm (based on intensity), a PDI of 0.239 and a zeta potential of  $-38.0 \pm 0.1$  mV. It can be seen from the TEM images that the nanoparticles were evenly dispersed without agglomeration ([Figure 1b](#)). The particle size observed from the TEM images was approximately 25 nm, which is similar with the size distributions based on number and volume ([Figure S1](#)). What's more, the characteristic peaks of potassium permanganate (at 315 and 545 nm) disappeared, and a broad UV absorption peak at 300–400 nm was observed for n-MO ([Figure 1c](#)), which is consistent with literature reports.<sup>40</sup>

n-MO is a nanozyme with ROS scavenging and oxygen producing activities. RDPP is a widely used fluorescence probe for oxygen detection and quantification. Due to dynamic quenching, molecular oxygen causes a significant decrease in the fluorescence of RDPP. Therefore, molecular oxygen can be detected by measuring the fluorescence intensity. As shown in [Figure S2](#), in the absence of n-MO, the fluorescence intensity of the RDPP solution remained nearly constant under both pH 7.4 and 4.0 condition, indicating that no oxygen was generated. As the concentration of H<sub>2</sub>O<sub>2</sub> increases, the fluorescence intensity decreases, indicating the production of more oxygen. Specially, in the groups containing n-MO, the fluorescence intensity showed a noticeable decrease. In the control group without H<sub>2</sub>O<sub>2</sub>, the fluorescence intensity at pH 4.0 decreased by approximately 21%, indicating that n-MO has some capacity to generate oxygen under acidic conditions. In the groups with added H<sub>2</sub>O<sub>2</sub>, the fluorescence intensity decreased obviously with increasing H<sub>2</sub>O<sub>2</sub> concentration, and the fluorescence intensity under the pH 4.0 group was lower than that under the pH 7.4 group. This suggests that the oxygen production catalytic ability of n-MO is positively correlated with both the H<sup>+</sup> concentration and H<sub>2</sub>O<sub>2</sub> concentration, which is consistent with the literature reports.<sup>40</sup> The results demonstrated that n-MO, with a nanozyme function, had been synthesized successfully.

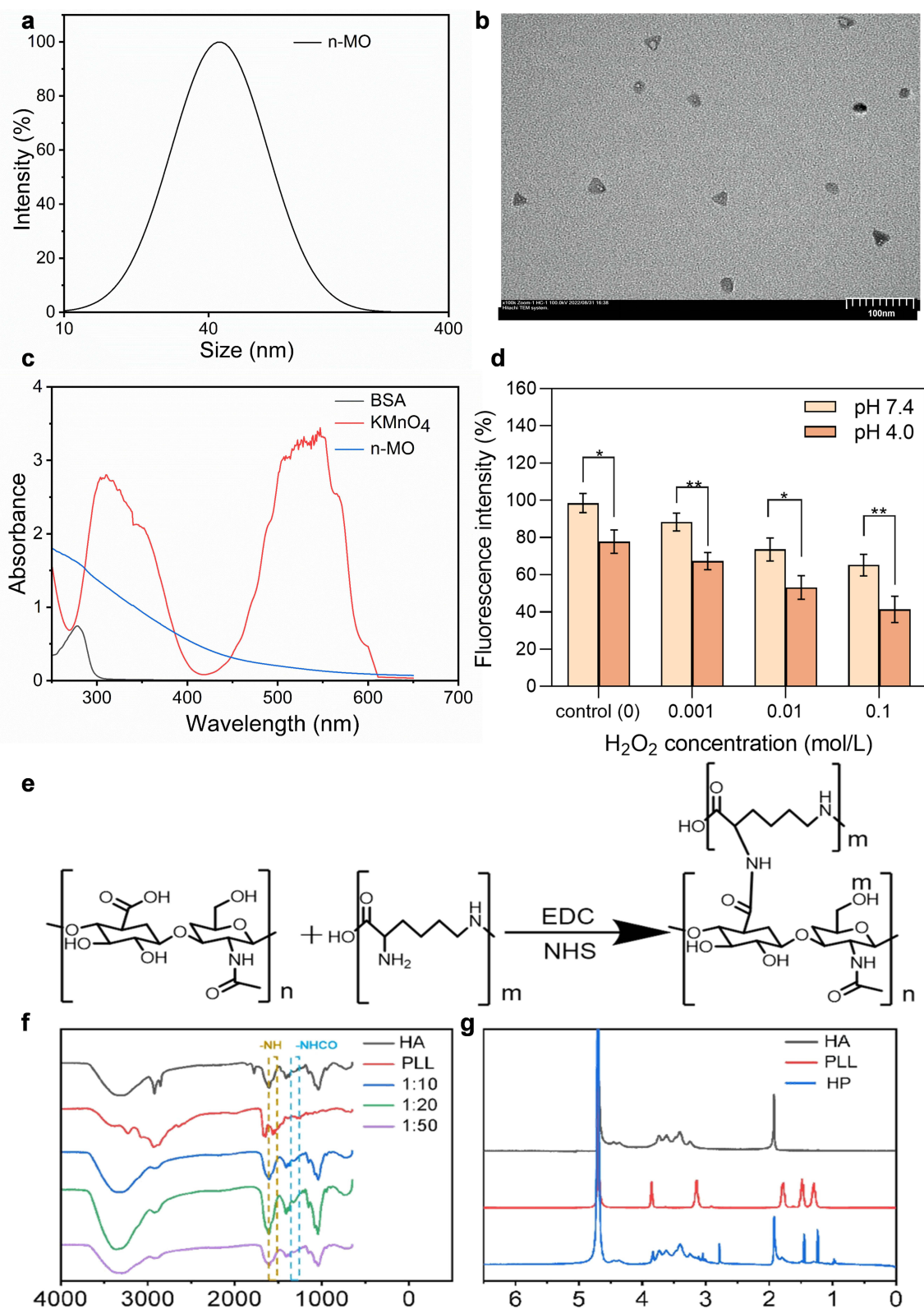


**Figure 1** Characterization of n-MO: (a) DLS analysis of particle size, (b) TEM images of n-MO, (c) UV absorption curves of BSA, KMnO<sub>4</sub>, and n-MO, (d) Oxygen production by different concentrations of n-MO in the presence of H<sub>2</sub>O<sub>2</sub> at different pH conditions (\**p*<0.05, \*\**p*<0.01, 95% CI). Synthesis and characterization of HA-PLL: (e) HA-PLL synthesis route, (f) IR spectra of HA, PLL, HP<sub>10</sub>, HP<sub>20</sub>, and HP<sub>50</sub>, (g) <sup>1</sup>H NMR spectra of HA, PLL, and HP<sub>20</sub>.



## Synthesis and Characterization of PLL Modified HA

The synthesis route of HA-PLL is shown in Figure 1e. Specifically, HA-PLL (HP) was synthesized by a carbodiimide coupling reaction between the carboxyl group of HA and the amino group of PLL. The molecular structures of HA, PLL and HP with different ratios of reactants were confirmed by ATR, as shown in Figure 1f. The peaks at  $3321\text{ cm}^{-1}$ ,  $1606\text{ cm}^{-1}$  and  $1407\text{ cm}^{-1}$  belonged to the stretching vibration of the carboxyl group of HA. In addition, the peaks at  $1158\text{ cm}^{-1}$ ,  $1077\text{ cm}^{-1}$ ,  $1034\text{ cm}^{-1}$  and  $949\text{ cm}^{-1}$  were characteristic peaks of polysaccharides. The adsorption peaks at  $1647\text{ cm}^{-1}$  and  $1566\text{ cm}^{-1}$  were attributed to vibrations of the peptide group, which were mainly generated by stretching vibrations of the C=O group and in-plane deformation vibrations of the N-H group of the amide bonds of PLL, respectively. In the HP spectrum, the peaks at  $1647\text{ cm}^{-1}$  and  $1566\text{ cm}^{-1}$  were replaced by a peak at  $1611\text{ cm}^{-1}$ . The appearance of a broad band between  $3000$  and  $3400\text{ cm}^{-1}$  was mainly due to the overlap of the carbonyl stretching vibration peak of PLL, the -NH stretching vibration peak of HA, and the formation of intramolecular or intermolecular hydrogen bonds. The intensity of the -NH absorption peak at  $1564\text{ cm}^{-1}$  in the HP spectrum was significantly lower than that in the PLL spectrum, indicating a decrease in the number of -NH<sub>2</sub> groups due to their reaction with carboxyl groups. Compared to the HA spectrum, the intensity of the amide bond (-CONH) at  $1320\text{ cm}^{-1}$  in the HP spectrum increased, indicating the formation of amide bonds during the reaction between PLL and HA. Moreover, the absorption peak of HP<sub>20</sub> was stronger than those of HP<sub>10</sub> and HP<sub>50</sub>, which suggested that HP<sub>20</sub> had the highest degree of crosslinking. Therefore, the optimal ratio of HA to PLL was 1:20, and HP<sub>20</sub> was used for hydrogel preparation.

Furthermore,<sup>1</sup>H NMR spectroscopy was performed to verify the structure and grafting rate of HP<sub>20</sub> (Figure 1g).<sup>41</sup> The characteristic peaks of PLL appeared at 3.8 ppm ( $\alpha$ -CH<sub>2</sub>), 1.95–1.35 ppm ( $\beta$ ,  $\gamma$ -CH<sub>2</sub>), and 2.9 ppm (NH-CH<sub>2</sub>). Additionally, the peaks from 3.0–4.0 ppm were assigned to the HA backbone. The grafting rate of HP<sub>20</sub> was quantified by comparing the integration of the peak of the vinyl group ( $\delta = 2.9$ ) with that of the HA backbone ( $\delta = 3.20$ – $4.20$ ) and was determined to be approximately 25%.

## Fabrication, Injectability and Morphology of MO-HPA Hydrogels

The scheme of hydrogel preparation is shown in Figure 2a. In situ hydrogels were formed by homogeneously mixing solution A and solution B, which transformed from a sol state to a gel state (Figure 2b). In the presence of Ca<sup>2+</sup>, sodium alginate generated calcium alginate and physically crosslinked with HP<sub>20</sub> to form hydrogels with a three-dimensional network structure. Generally, the structures of MO-HPA hydrogels were fabricated by the combination of chemical crosslinking (carboxyl group of HA and the amino group of PLL) and physical crosslinking (HP with alginate), as well as ionic crosslinking (alginate with Ca<sup>2+</sup>). Considering the high viscosity of the polymer solution, its syringe ability was investigated. Solution A (containing HP and SA) was easily injected into solution B through a narrow 23G needle, and the mixture rapidly formed a gel (Figure 2a). These results indicated that the hydrogel precursor solutions had satisfactory syringe ability and formability, which are beneficial for clinical application.

The micromorphology of the lyophilized hydrogels (MO-HPA<sub>0.5</sub>, MO-HPA<sub>1.0</sub>, and MO-HPA<sub>1.5</sub>) was observed by SEM. According to the SEM images, all of the hydrogels exhibited a uniform dense network with a highly porous structure, the diameters of which were approximately 50  $\mu\text{m}$  (Figure 2c). Moreover, the HP<sub>20</sub> concentration played an important role in the microstructure of the gel. With an increasing concentration of HP<sub>20</sub>, the hydrogels became more homogeneous and denser. Specifically, the order of homogeneity and crosslinking density of the hydrogels is MO-HPA<sub>1.5</sub> > MO-HPA<sub>1.0</sub> > MO-HPA<sub>0.5</sub>. Notably, there is a close relationship between the micromorphology and adaptability of the hydrogels. The homogeneous structure of the gels might be attributed to their mechanical properties.<sup>42</sup> Moreover, hydrogels with similar microstructures would be beneficial for the diffusion and exchange of nutrients, oxygen, and other biomolecules, which implies that they could be further applied for cell proliferation and tissue engineering.

Notably, the materials used to synthesize MO-HPA hydrogels are readily available and relatively cost-effective, which supports the potential for large-scale production. The in situ gelation process is straightforward and can be adapted to a clinical setting, enabling ease of application. Moving forward, our study would focus on optimizing production techniques to ensure consistency in properties, such as mechanical strength and gelation time, to meet regulatory standards for medical use.

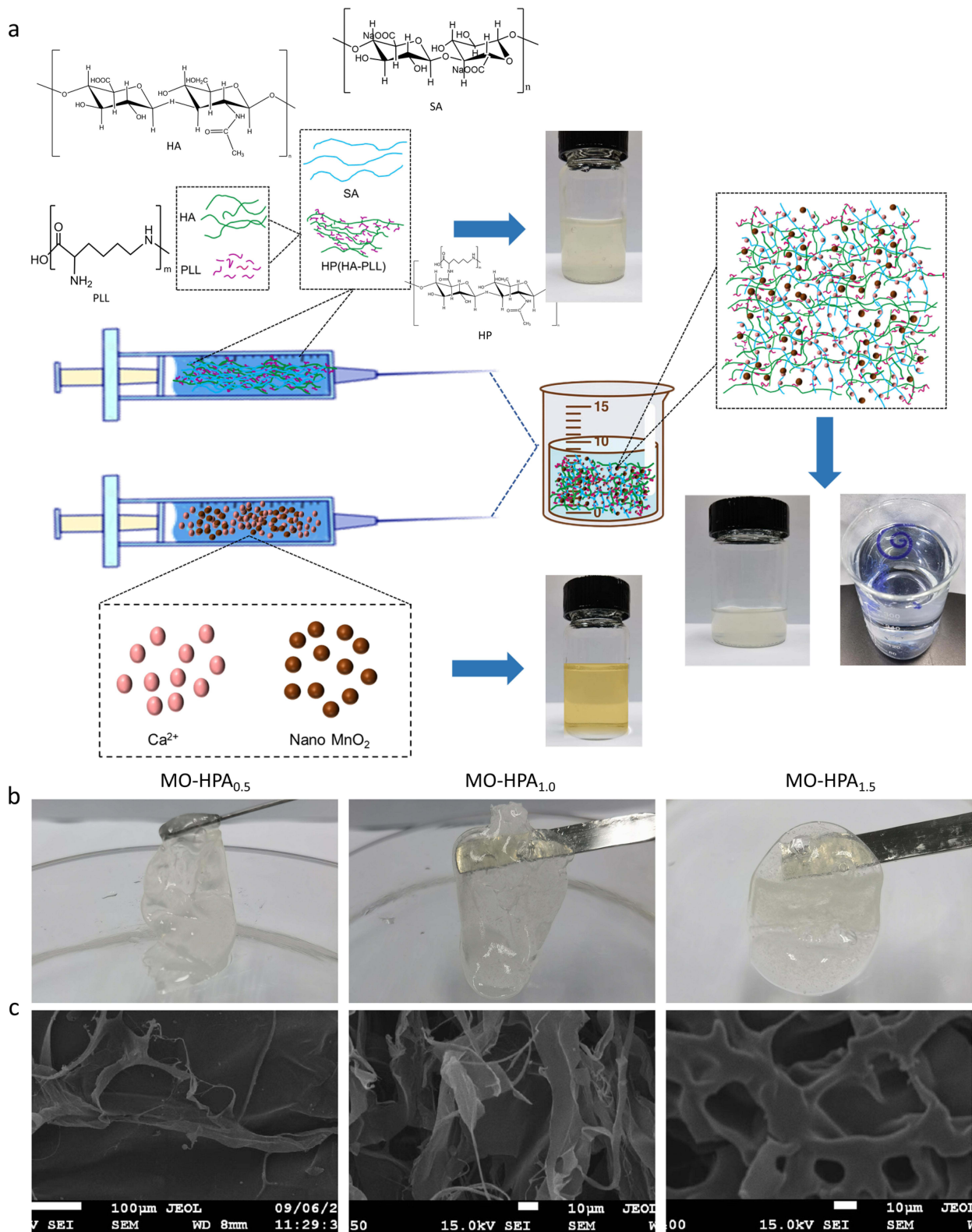


**Figure 2** Preparation and characterization of the hydrogels. (a) Scheme of hydrogel preparation. (b) Appearance and (c) Internal morphology of the hydrogel with different polymer concentrations.

## Gelation Time, Swelling Properties, and Self-Healing Properties

The gelation time was determined by the vial tilting method. As shown in Figure 3a, the sol–gel transformation of MO-HPA with different HP<sub>20</sub> concentrations took place in 65 seconds. However, the gelation time of MO-HPA decreased as the HP<sub>20</sub> concentration increased, and MO-HPA<sub>1.5</sub> showed the shortest gelation time. The accelerated formation of the hydrogels may be caused by increased chain entanglement between HP<sub>20</sub> and alginate. It is worth noting that the gelation time is influenced by temperature; as the temperature decreases, the time required for gel formation increases. Considering that parts of tube was positioned on the surface of the skin, the gelation experiment was conducted at room temperature (around 25°C). The equilibrium swelling ratio is an important parameter to evaluate the crosslinking degree. As shown in Figure 3b, all of the hydrogels with various HP<sub>20</sub> contents reached swelling equilibrium within 300 s. The water content of MO-HPA<sub>1.0</sub> was relatively higher, which may be due to it being more porous than MO-HPA<sub>0.5</sub> and having a lower crosslinking density than MO-HPA<sub>1.5</sub>, which are conducive to the permeation of water molecules. According to the literature, hydrogels with excellent absorbability are beneficial for absorbing excess exudate.<sup>43</sup>

The in situ hydrogel molding characteristics were thus further evaluated. As shown in Figure 3c, the letters “UJS” could be written on the hydrogel without difficulty. Moreover, the letter “J” written on all the MO-HPA hydrogels could be lifted, indicating the potential mechanical strength of the hydrogels. The macroscopic self-healing ability of the MO-HPA hydrogels was further detected. As shown in Figure 3d, the two semi-blocks (MO-HPA<sub>1.0</sub>), stained or not with bromophenol blue, started to close in several minutes and completely merged into an intact hydrogel, which was likely due to reversible physical crosslinking and ionic crosslinking. This self-healing property ensured that the hydrogels could reform if they were destroyed accidentally from the daily tube movement or wound contact after gastrostomy. These results indicated that the multivariate crosslinking system endowed the MO-HPA hydrogels with adaptability, moldability and self-healing characteristics that could match the complex environments of gastrostomy wounds.

## Cytotoxicity Test and Fibroblast Migration

Biocompatibility and biosafety are important prerequisites for the clinical application of hydrogels. MTT and hemolysis assays were performed to evaluate cell and blood compatibility. 3T6-Swiss albino cells were used as model cells to assess the cytotoxicity of the n-MO and MO-HPA hydrogels. As shown in Figure 4a, the viabilities of cells treated with various concentrations of n-MO were almost over 80% after incubation for 24, 48 or 72 h, which indicated that n-MO has good safety within the concentration range tested. The toxicity of the MO-HPA hydrogels to 3T6-Swiss albino cells was also assessed at 24, 48 and 72 h. As shown in Figure 4b-d, cell viability remained over 80% during cocultivation, exhibiting the good cytocompatibility of the hydrogels. Moreover, the viability values in some groups were even greater than 100%, which may be because HA promotes cell proliferation. It was reported hyaluronic acid is a major component of the extracellular matrix, capable of regulating the secretion of growth factors and cytokines, and influencing cell adhesion, growth, proliferation, and differentiation.<sup>44</sup> Alginate can serve as a synthetic extracellular matrix material and promotes the proliferation of fibroblasts.<sup>45</sup> Thus, this phenomenon was consistently observed in multiple experiments and is also indicative of hyaluronic acid and alginate’s biocompatibility.

Fibroblasts play a crucial role in the replacement of damaged ECM and the promotion of tissue healing. During this process, the migration and proliferation of fibroblasts to the injury site remodel the surrounding microenvironment and promote tissue regeneration. A scratch test was performed with 3T6 cells to determine whether the MO-HPA hydrogel can promote the migration of fibroblasts. As shown in Figure 4e and f), compared to the control group, the cell migration rates of the three MO-HPA hydrogel groups (MO-HPA<sub>0.5</sub>, MO-HPA<sub>1.0</sub>, and MO-HPA<sub>1.5</sub>) were increased by approximately 12.3%, 17.0% and 23.3%, respectively. The MO-HPA<sub>1.5</sub> group displayed the highest cell migration rate (about 41.3%). These results indicated that as the proportion of HP<sub>20</sub> in the hydrogels increased, the gel’s ability to promote cell proliferation was also enhanced.

## Cellular Oxygen Production

The principle of n-MO catalysis of H<sub>2</sub>O<sub>2</sub> to generate oxygen is shown in Figure 5a. Oxygen is crucial for collagen synthesis, angiogenesis, and tissue regeneration. Local wound hypoxia due to poor oxygen diffusion and permeation

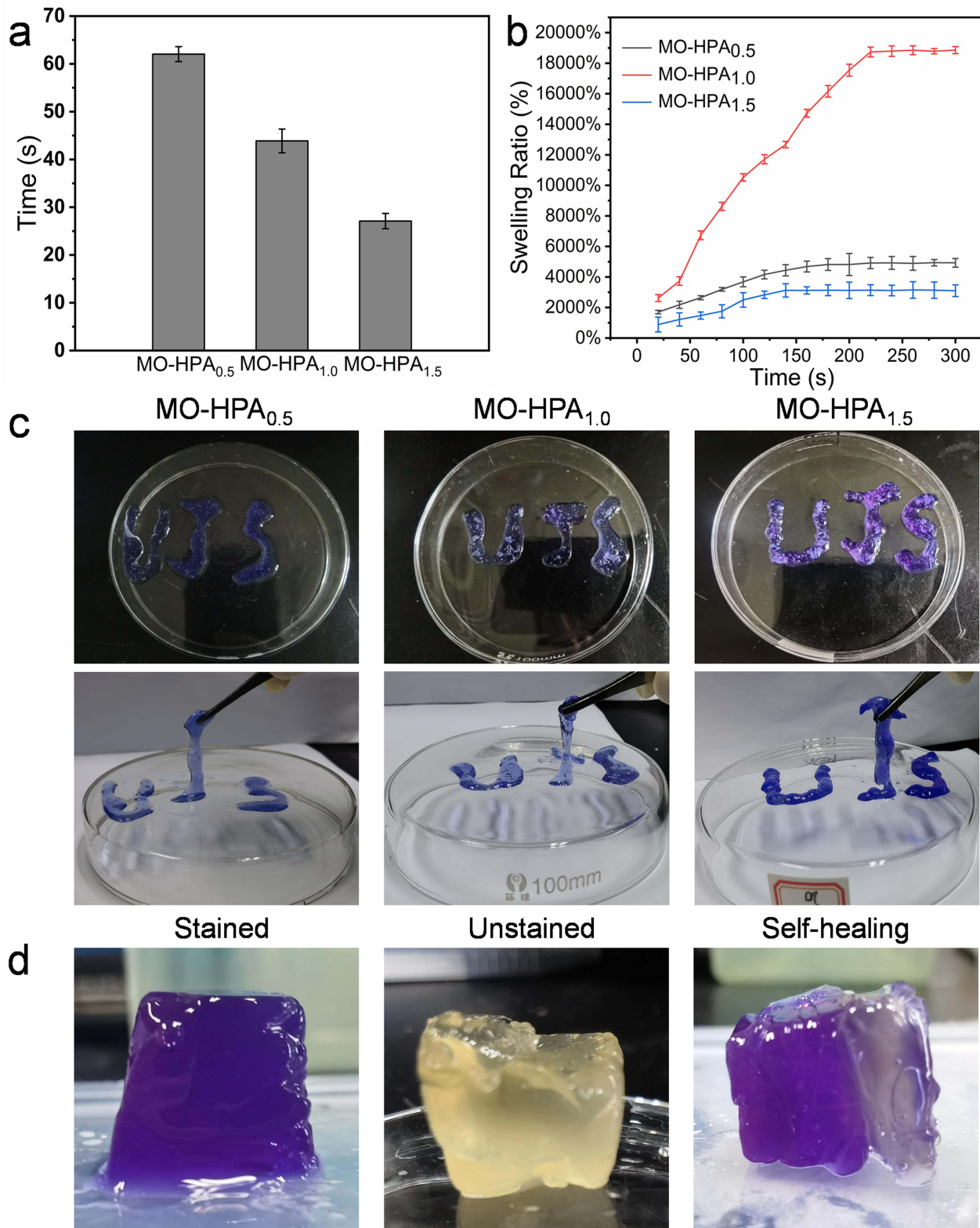


**Figure 3** Characterization of the hydrogels. (a) Gelation times and (b) Swelling ratios of hydrogels with different polymer concentrations. (c) Injectability and (d) Self-healing properties of the hydrogels.

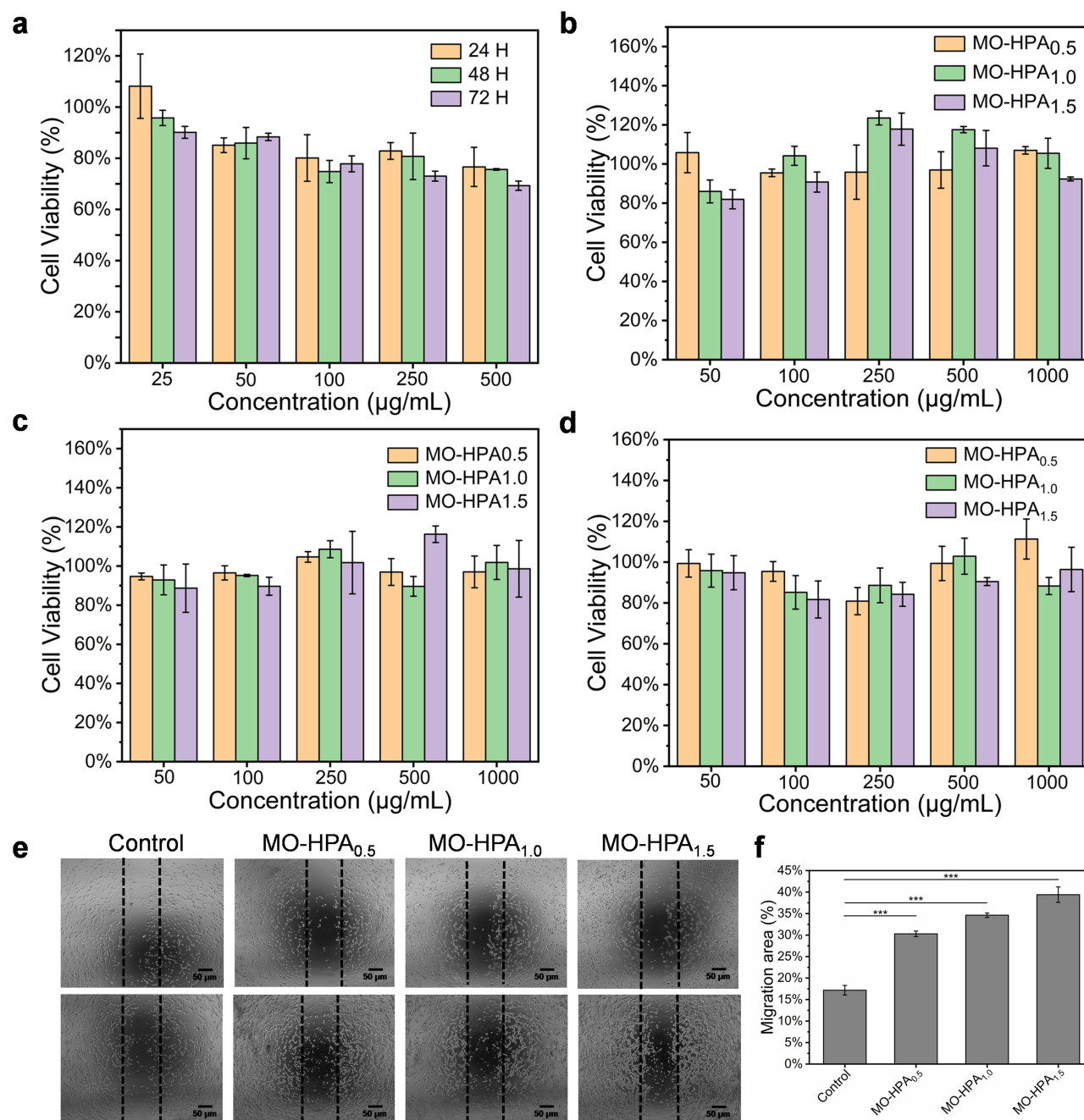


**Figure 4** (a) Viabilities of 3T6 cells treated with various concentrations of n-MO for 24, 48, and 72 h. (b-d) Viabilities of 3T6 cells after incubation in various concentrations of MO-HPA for 24 h, 48 h and 72 h. (e) Fibroblast migration behaviors and (f) rates after treatment with different concentrations of hydrogels (\*\*\* $p < 0.001$ , 95% CI). Scale bars represent 100 µm.

affect the healing process. The n-MO in MO-HPA<sub>1.0</sub> is a nanozyme with oxygen producing activities. The ability of MO-HPA<sub>1.0</sub> to mimic CAT activity and catalyze the conversion of H<sub>2</sub>O<sub>2</sub> to O<sub>2</sub> was investigated under pH 1.5, 4.0 and 7.4 conditions, simulating fasting, postprandial gastric conditions and physiological conditions, respectively, *in vitro* experiments. RDPP served as a luminescent indicator for oxygen detection, with molecular oxygen leading to a reduction in fluorescence intensity of RDPP through a dynamic quenching process. In that case the fluorescence intensity inversely correlates with the amount of O<sub>2</sub> produced, with higher reductions in fluorescence indicating greater O<sub>2</sub> output. As shown in Figure 5b, the fluorescence intensities of the HPA<sub>1.0</sub> hydrogels in the groups without n-MO were almost unchanged under all pH conditions. Notably, the MO-HPA<sub>1.0</sub> hydrogel groups with H<sub>2</sub>O<sub>2</sub> reduced the fluorescence intensities under

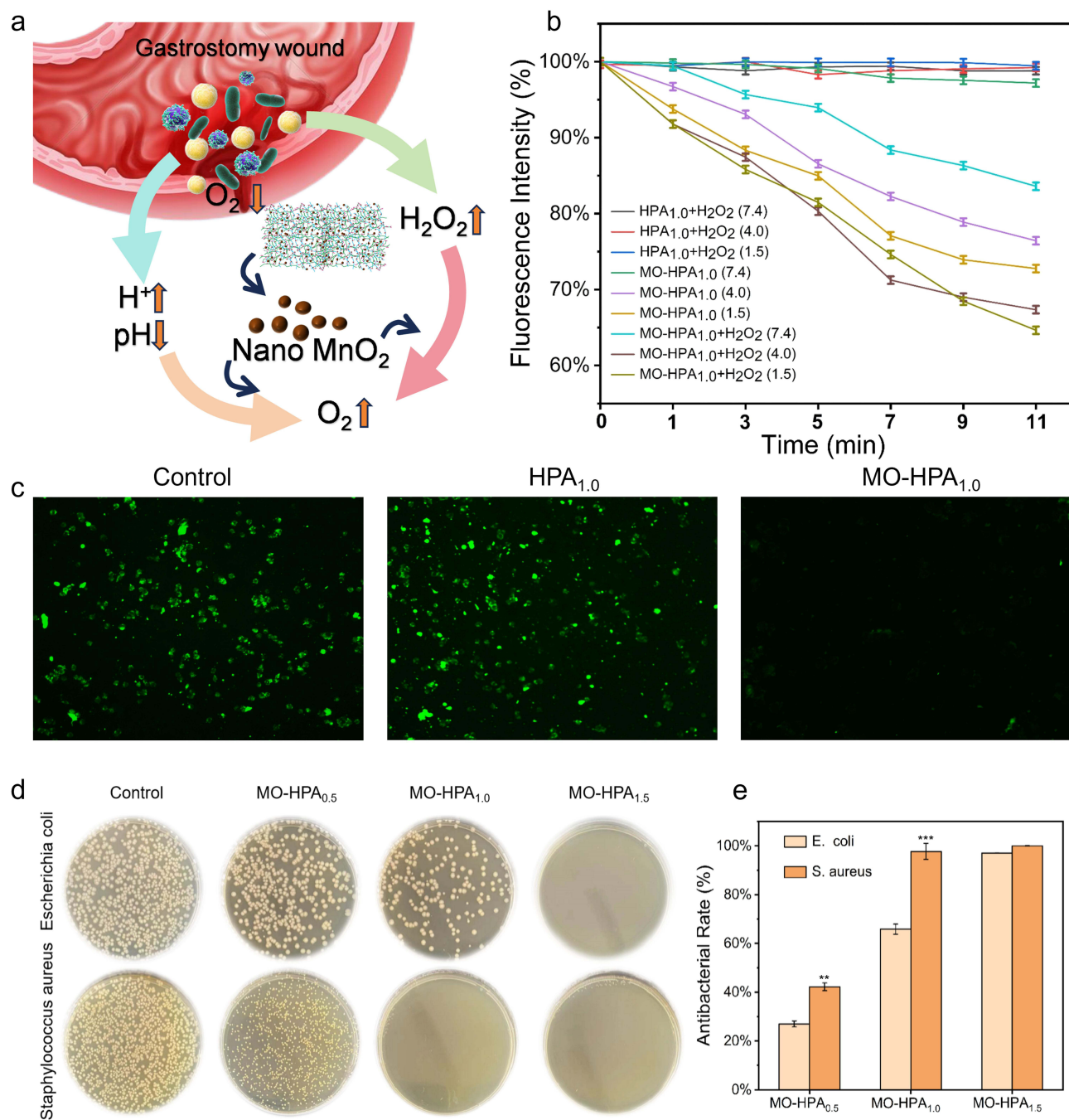


**Figure 5** (a) The principle of n-MO catalysis of H<sub>2</sub>O<sub>2</sub> to generate oxygen. (b) Fluorescence intensity of NIH-3T6 cells treated with HPA hydrogels with or without n-MO. (c) Fluorescence intensity of NIH-3T6 cells treated with HPA hydrogels with or without n-MO. (d) Antibacterial effects of MO-HPA hydrogels against *S. aureus* and *E. coli*. (e) Quantitative evaluation of the antibacterial effects of the MO-HPA hydrogels (\*\**p*<0.01, \*\*\**p*<0.001, 95% CI).

acidic conditions (pH 1.5 and 4.0) remarkably. These results indicated that, in the presence of H<sub>2</sub>O<sub>2</sub>, the MO-HPA<sub>1.0</sub> hydrogel showed a stronger ability to remove H<sub>2</sub>O<sub>2</sub> and promote oxygen production, especially in the presence of H<sup>+</sup>, which is beneficial for applications to gastrostomy wounds in acidic conditions. Well, in the absence of H<sub>2</sub>O<sub>2</sub>, the MO-HPA<sub>1.0</sub> hydrogel had no oxygen production under physiological condition, but a little oxygen production capacity under acidic conditions, which was due to the ability of n-MO to use H<sup>+</sup> to produce oxygen.

The catalytic ability of the MO-HPA<sub>1.0</sub> hydrogels was further evaluated in NIH-3T6 cells under hypoxic conditions. As shown in Figure 5c, the control group and HPA<sub>1.0</sub> hydrogel group had notable and similar fluorescence intensities,

suggesting that the HPA<sub>1.0</sub> hydrogel without n-MO lacked the ability to regulate the intracellular oxygen content. However, the fluorescence intensity in the cells treated with MO-HPA<sub>1.0</sub> was significantly decreased, indicating n-MO in the gel elevated intracellular oxygen content. It is thus suggested that MO-HPA<sub>1.0</sub> was able to regulate the oxygen balance in hypoxic cells via its CAT-mimicking activity.

## Antibacterial Ability

The antibacterial effects of the MO-HPA hydrogels against *S. aureus* and *E. coli* were evaluated by spread plate assays. As shown in Figure 5d, the numbers of bacterial colonies (including *S. aureus* and *E. coli*) treated with the MO-HPA hydrogels were significantly reduced compared with the control group, which indicated that the MO-HPA hydrogels possessed antibacterial effects against both gram-positive and gram-negative bacteria. Moreover, for *E. coli*, the antibacterial efficiency of the MO-HPA<sub>1.0</sub> and MO-HPA<sub>1.5</sub> groups increased by 40.1% and 73.4%, respectively, compared to the MO-HPA<sub>0.5</sub> group. Similarly, for *S. aureus*, the antibacterial efficiency of the MO-HPA<sub>1.0</sub> and MO-HPA<sub>1.5</sub> groups increased by 55.6% and 57.6%, respectively, compared to the MO-HPA<sub>0.5</sub> group. These results indicated that the antibacterial efficiency of the hydrogels was enhanced with increasing HP<sub>20</sub> concentration, and MO-HPA<sub>1.5</sub> exhibited the strongest inhibitory effect (Figure 5e). The potential antibacterial mechanism of the MO-HPA hydrogels was considered to be the inhibition and killing effect of PLL due to its ability to change the bacterial membrane permeability and the electrostatic interactions between  $-\text{NH}_3^+$  and the functional groups on the bacterial membrane surface.<sup>46</sup>

## Rheological and Mechanical Properties

The compressive properties of the MO-HPA hydrogels were further evaluated. As shown in Figure 6a, the strength of the hydrogels increased with increasing compressive force in the initial stage, indicating that all the MO-HPA hydrogels possessed appropriate compressive properties. Specifically, the compressive stress of MO-HPA<sub>0.5</sub> hydrogel was approximately 0.011 MPa. With the increase of the concentration of HP<sub>20</sub>, the compressive stress of MO-HPA<sub>1.0</sub> hydrogel and MO-HPA<sub>1.5</sub> hydrogel improved to around 0.016 MPa and 0.015 MPa, respectively, indicating an enhancement the mechanical properties for wound healing application.<sup>25</sup> Porcine skin tensile experiments were performed to evaluate the adhesion properties of the MO-HPA hydrogels. As shown in Figure 6b, the adhesion of the M-HPA<sub>0.5</sub>, MO-HPA<sub>1.0</sub> and MO-HPA<sub>1.5</sub> hydrogels to fresh porcine skin increased with increasing HP<sub>20</sub> concentration to approximately 0.13 Mpa, 0.35 Mpa and 0.48 Mpa, respectively. The potential mechanism was considered to be the presence of the  $-\text{NH}_2$  group in PLL, which could form hydrogen bonds with the H<sub>2</sub>O in porcine skin. In general, adhesive hydrogels are favorable for effective binding to tissue, which is beneficial for biomedical usage.

Dynamic rheological tests, including time sweep, dynamic strain sweep, frequency sweep and stress relaxation tests, were performed on the MO-HPA hydrogels to evaluate their viscoelastic characteristics. As shown in Figure 6c, the time oscillation scanning curves showed that the energy storage moduli ( $G'$ ) of MO-HPA<sub>1.0</sub> and MO-HPA<sub>1.5</sub> were higher than their loss moduli ( $G''$ ). The  $\tan \delta$  ( $G''/G'$ ) values of MO-HPA<sub>1.0</sub> and MO-HPA<sub>1.5</sub> were less than 1.0, which indicated that they act as viscoelastic gels. However, for the MO-HPA<sub>0.5</sub> hydrogel,  $G'$  was close to  $G''$ , suggesting poor mechanical properties compared with those of MO-HPA<sub>1.0</sub> and MO-HPA<sub>1.5</sub>. The shear thinning behaviors of the MO-HPA hydrogels with different HP<sub>20</sub> concentrations were further examined. As shown in Figure 6d, the viscosity of all the MO-HPA hydrogels decreased with increasing shear rate, which demonstrated shear thinning behavior and good injectability. The frequency sweep curves of all MO-HPA hydrogels showed that both  $G'$  and  $G''$  increased with increasing frequency, and the value of  $G'$  was larger than that of  $G''$  in the frequency range of 0.01–10 Hz (Figure 6e). These results indicated that the MO-HPA hydrogels have a stable structure and viscoelasticity, presumably due to physical entanglement in the chemically crosslinked network.<sup>17,47</sup> These rheological characteristics indicated that the MO-HPA hydrogels with tunable viscoelasticity is beneficial for meeting the demands of clinical applications.

The gel-sol transition point and linear viscoelastic region of the MO-HPA hydrogels were detected by strain sweep and frequency sweep tests. As shown in Figure 6f,  $G'$  was higher than  $G''$  at 70% strain in the sweep curves, indicating the stable structure of the hydrogel. However, as the shear strain increased,  $G''$  gradually exceeded  $G'$ , implying a gel-to-

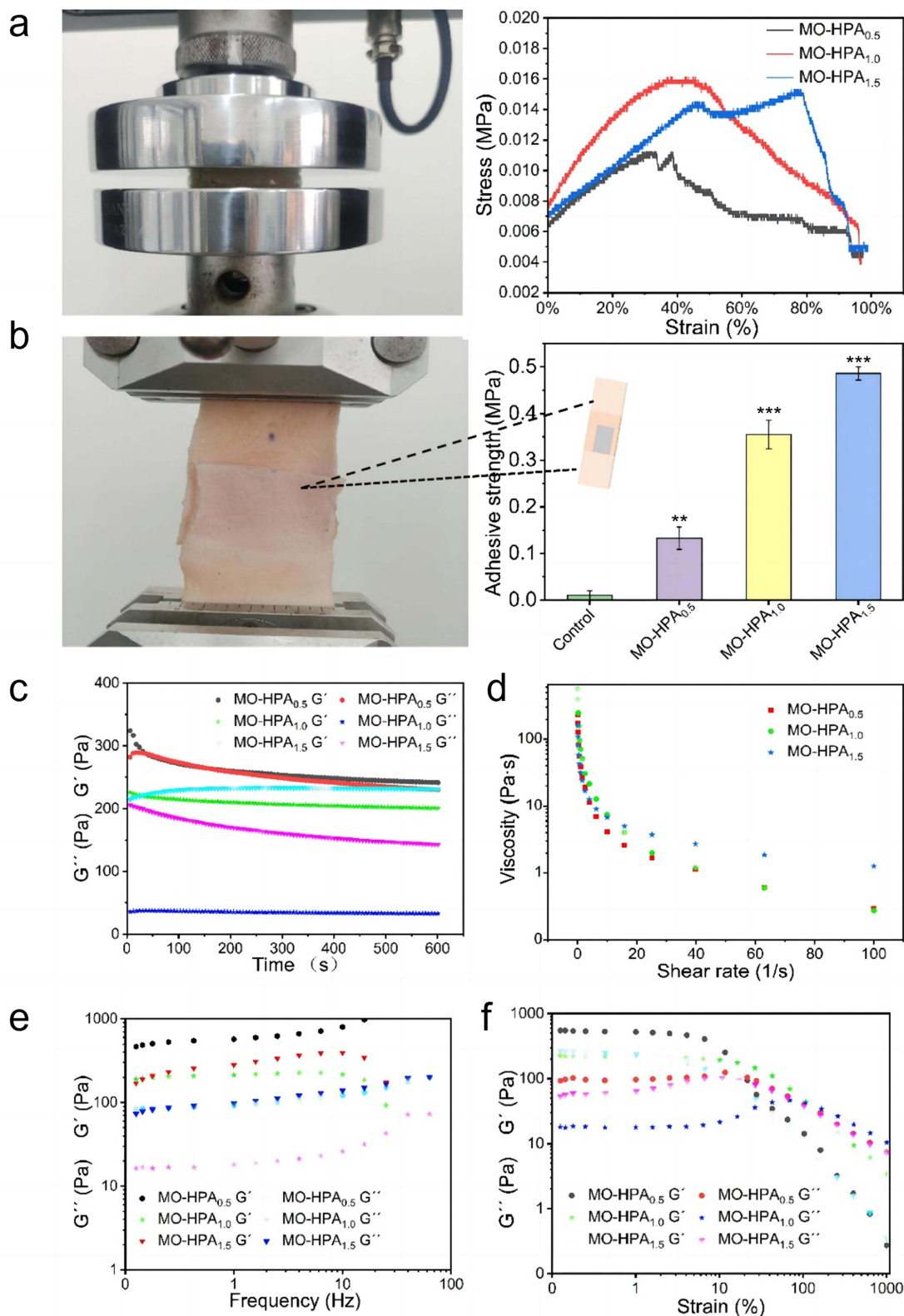


**Figure 6** Rheological properties and mechanical properties of the MO-HPA hydrogels. (a) Compression test. (b) Skin adhesion and tensile test (\*\* $p < 0.01$ , \*\*\* $p < 0.001$ , 95% CI). (c) Time oscillation scan. (d) Shear viscosity. (e) Frequency scan. (f) Strain amplitude scan.



sol phase transition. Notably, MO-HPA<sub>1.0</sub> exhibited a postponed transformation point in the curve, indicating a more stable network.

Considering that it had the best water absorption performance, the most stable internal structure, and appropriate mechanical properties, MO-HPA<sub>1.0</sub> was therefore used for subsequent research.

## Blood Compatibility Evaluation

The blood compatibility of the hydrogels was further proven by hemolysis experiments. As shown in Figure 7a, the positive control group was bright red, indicating the rupture of blood cells. However, all the hydrogel groups were almost colorless and transparent and consistent with the negative control group. This conclusion was also confirmed by UV full-wavelength scanning of the supernatants from all groups (Figure 7b). Cell morphology is shown in Figure 7c. It was visually evident that almost all of the red blood cells in the positive group had ruptured, while those of the hydrogel group maintained an intact morphology. These results indicated that the hydrogels possessed good blood compatibility and do not carry a risk of hemolysis.

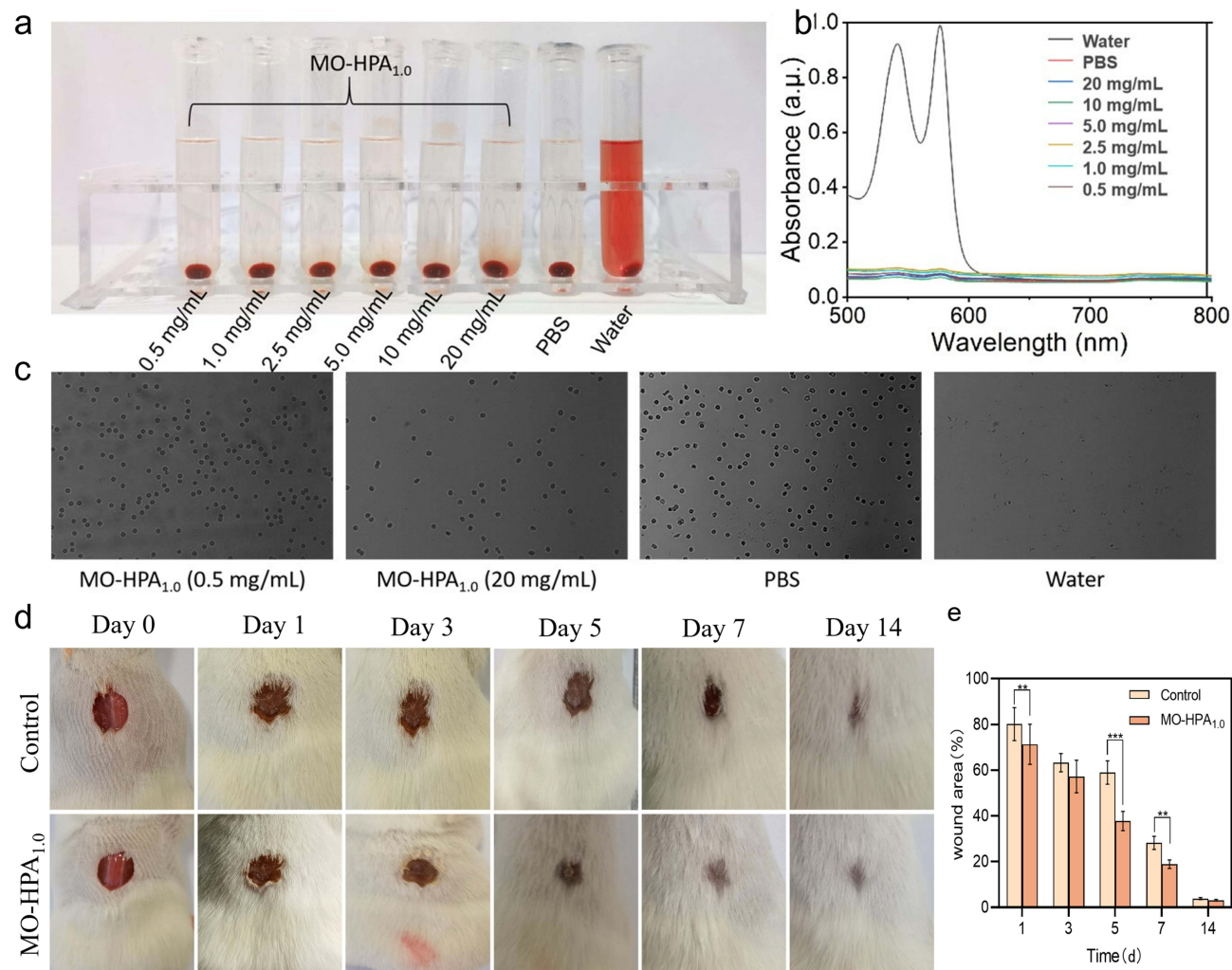


**Figure 7** Visual illustration (a) of the hemolysis assay and UV absorption curves (b) of the supernatant fluids. (c) Morphologies of red blood cells under microscope (20 ×). (d) wound healing area treated with normal saline and MO-HPA<sub>1.0</sub> hydrogels on Days 0, 1, 3, 5, 7 and 14 (\*\**p*<0.01, \*\*\**p*<0.001, 95% CI). (e) Representative images of mouse wounds.

## Healing of Mouse Full-Thickness Skin Defects

A mouse dorsal full-thickness skin defect model was established to preliminarily evaluate the effect of the MO-HPA<sub>1.0</sub> hydrogel on wound healing. The in situ hydrogel formed rapidly on the wounds of the mice after injection. Representative images of the wound areas treated with normal saline (control group) and MO-HPA<sub>1.0</sub> hydrogels on Days 0, 1, 3, 5, 7 and 14 are shown in [Figure 7d](#). Both groups showed a continuous reduction in wound area. Notably, the MO-HPA<sub>1.0</sub> hydrogel-treated groups showed nearly complete wound healing on the 7<sup>th</sup> day, while the control group still exhibited obvious blood clot scabs in the epidermis. Specially, as shown in [Figure 7e](#), on day 7, the wound area ratio of the control and MO-HPA<sub>1.0</sub> treatment groups were approximately 28.2% and 18.9%, respectively ( $p < 0.01$ ), indicating the treatment effect of MO-HPA<sub>1.0</sub> group was significantly better than that of control group. These results suggested that the MO-HPA<sub>1.0</sub> hydrogel had the ability to promote wound treatment.

## Acceleration of Tract Maturation in the Rabbit Gastrostomy Model

A rabbit gastrostomy model was established to further investigate the effect of the MO-HPA<sub>1.0</sub> hydrogels on tract maturation after gastrostomy. We successfully constructed a rabbit gastrostomy model by adopting surgical methods, following improvements as reported in the literature.<sup>48</sup> This method does not require the use of an endoscope and is beneficial for completion in the laboratory. Additionally, the gastrostomy rabbits can survive well during the experimental period. As shown in [Figure 8a](#), a mature tract along the tube between the gastric and abdominal walls formed in the MO-HPA<sub>1.0</sub> hydrogel group on approximately the 7<sup>th</sup> day after gastrostomy. However, the control group only began to develop a new tract on the tube in proximity to the peristomal site on the 7th day. Tract maturation in the control group was observed 14 days after gastrostomy, while at this time, a compact connection between the stomach and the abdominal wall had formed on the peristomal site in the MO-HPA<sub>1.0</sub> hydrogel group.

Blood vessels, collagen, and myogenic fibers play important roles in tissue healing. H&E and Masson staining were performed to evaluate tissue healing of the peristomal site wounds after gastrostomy. As shown in [Figure 8b](#), the MO-HPA<sub>1.0</sub> hydrogel group showed much many more glands (yellow arrows) and fibroblasts (black arrows) than the control group on Day 7, indicating the angiogenic effect of the hydrogel. Likewise, as shown in [Figure 8c](#) and [e](#), on day 7, the collagen content in the control group was approximately 33.2%, whereas the hydrogel group exhibited a collagen content of about 46.9%, indicating a significant increase in the accumulation of collagen in the dermis ( $P < 0.001$ ). Additionally, the expression level of HIF-1 $\alpha$  in the MO-HPA<sub>1.0</sub> hydrogel group significantly decreased ( $P < 0.001$ ), reaching only 30.9% of that in the control group on day 7 ([Figure 8d](#) and [f](#)). The level of HIF-1 $\alpha$  reflects the hypoxia degree of the wound tissue. The results indicated that the gel downregulated HIF-1 $\alpha$  and ameliorate hypoxic conditions. In general, after treatment with the MO-HPA<sub>1.0</sub> hydrogels, micro-vessels and collagen fibers were visible in the regenerated mature tract tissue 7 days post gastrostomy, demonstrating excellent injury healing and tissue regeneration effects of the hydrogel. The levels of inflammatory cytokines, including TNF- $\alpha$ , IL-6 and IL-1 $\beta$  were also evaluated. As shown in [Figure S3](#), compared to the control group, the levels of TNF- $\alpha$ , IL-6 and IL-1 $\beta$  were significantly decreased on day 7 and day 14 ( $p < 0.01$ ). The results suggested that treatment with MO-HPA<sub>1.0</sub> effectively reduced the levels of the inflammatory cytokines TNF- $\alpha$ , IL-1 $\beta$ , and IL-6 in wound environments.

These results indicated that the MO-HPA<sub>1.0</sub> hydrogels effectively accelerated tract maturation, which may be conducive to reducing clinical risks, such as free perforation, abdominal infection, and difficulty in reinsertion after accidental catheter detachment. Current wound dressings, including conventional hydrogels, face challenges in treating gastrostomy-related wounds due to their inability to effectively address hypoxia or control the oxidative environment at the wound site. Moreover, most existing hydrogel treatments do not possess the necessary antimicrobial properties to prevent infection in such highly exposed wounds. The MO-HPA hydrogel, with its unique oxygen-generating capabilities and ROS modulation, offers an innovative solution that addresses both hypoxia and bacterial contamination, representing a novel approach in the management of gastrostomy-related wounds.

The multifunctional MO-HPA hydrogels developed in this study exhibit antibacterial, hypoxia-relieving, and proliferative properties, which make them suitable for clinical situations beyond gastrostomy wound management. Given the increasing prevalence of multidrug-resistant infections, these hydrogels could offer an effective, non-antibiotic approach

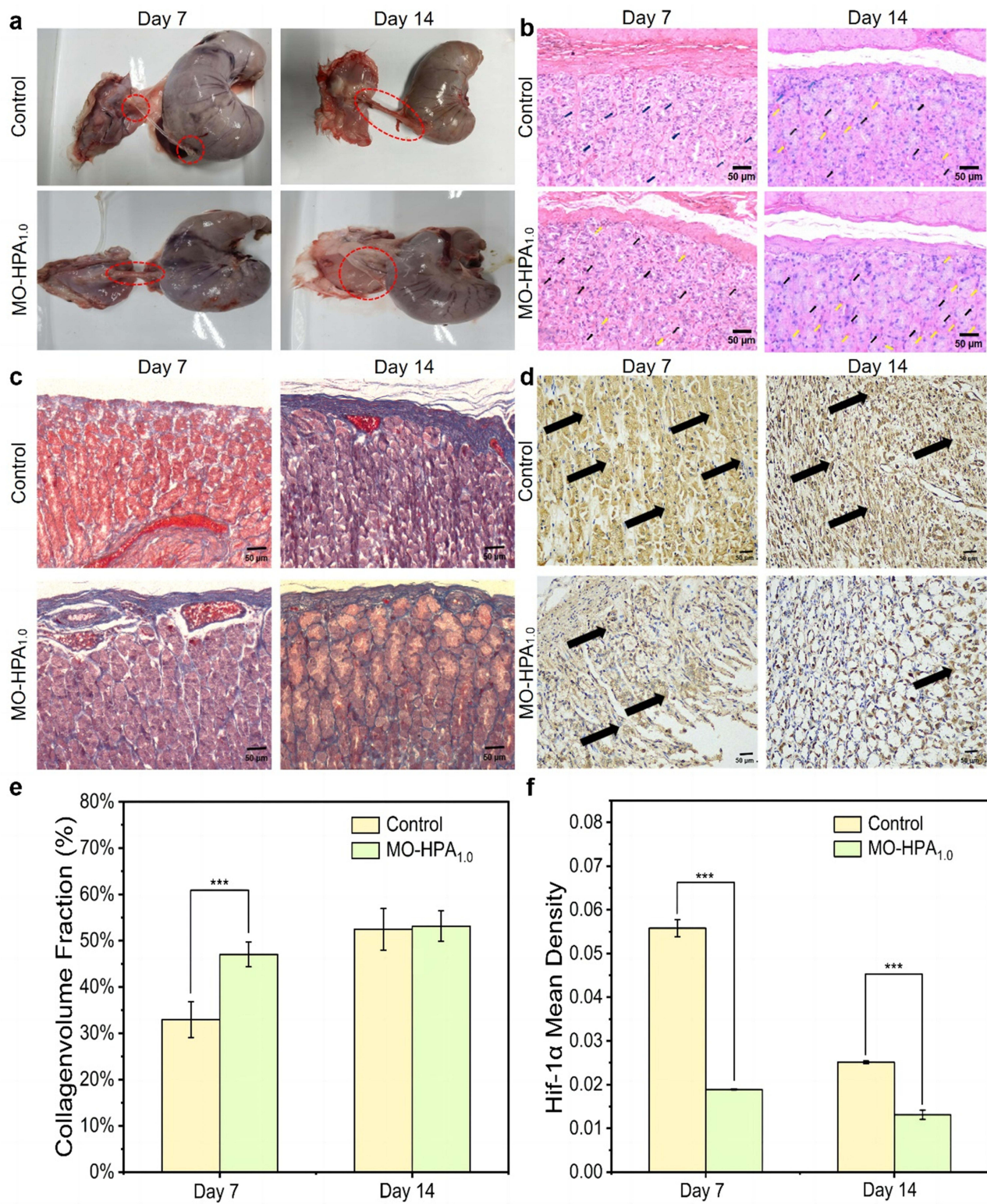


**Figure 8** (a) Macroscopic evaluations of tract maturation in the rabbit gastrotomy model at days 7 and 14. (b) HE staining images (black arrows: fibroblasts; yellow arrows: glands). (c) and (d) Masson staining and HIF-1 $\alpha$  staining of gastrotomy wound sections 7 and 14 days after treatment. The scale bars are 50  $\mu$ m. (e) and (f) Collagen fraction and HIF-1 $\alpha$ -positive density of gastrotomy wound tissues after various treatments through Masson staining or immunohistochemical staining. (\*\*\*) $p < 0.001$ , 95% CI).

to managing chronic wounds, such as diabetic ulcers, pressure sores, chronic non-healing wounds. These wounds often remain in a persistent inflammatory state and suffer from poor oxygenation, similar to gastrostomy wounds. The antimicrobial capabilities of MO-HPA, coupled with its ability to scavenge ROS and hypoxia-relieving, indicate its potential use in treating these complex wound environments. Future studies could focus on evaluating the efficacy of MO-HPA hydrogels in such chronic wound models, thereby expanding its clinical relevance and impact.

Additionally, the main components of the hydrogel, such as hyaluronic acid and sodium alginate, are well-known for their biodegradability, primarily via enzymatic pathways that ensure their breakdown into biocompatible by-products.<sup>49,50</sup> Although the short-term efficacy of MO-HPA hydrogels has been demonstrated in our study, the long-term implications is critical for clinical translation. In future research, the long-term tissue compatibility, potential immune responses of the hydrogel will be evaluated to further support its clinical translation and application.

## Conclusion

In this study, the injectable, nanozyme-based, multifunctional in situ hydrogels (MO-HPA) with antibacterial properties, ROS scavenging, and oxygen production capabilities were successfully developed. The hydrogel significantly reduced inflammatory factors and promoted collagen synthesis and fibroblast migration, which are beneficial for wound healing and gastrostomy tract maturation. It is worth noting that, at present, there is still a lack of research on promoting peristomal site wound treatment and tract maturation after gastrostomy. This study is the first to carry out research on promoting tract maturation after gastrostomy through the use of in situ hydrogels, which has important significance and application value for reducing the complications of gastrostomy. Furthermore, the hydrogel's unique properties suggest that it could be valuable in treating chronic wounds characterized by hypoxia and persistent inflammation, such as diabetic ulcers and pressure sores, highlighting its potential for broader wound care applications. Additionally, the potential long-term effects, biodegradability, and manufacturing scalability of the hydrogel will be explored in future studies to ensure its suitability for prolonged clinical use.

## Acknowledgments

This work was supported by National Natural Science Foundation of China (No.82172042), Shanghai Municipal Health Commission (202140077) and Shanghai Municipal Health Commission (20224Y0301).

## Author Contributions

All authors made a significant contribution to the work reported, whether that is in the conception, study design, execution, acquisition of data, analysis and interpretation, or in all these areas; took part in drafting, revising or critically reviewing the article; gave final approval of the version to be published; have agreed on the journal to which the article has been submitted; and agree to be accountable for all aspects of the work.

## Disclosure

The authors report no conflicts of interest in this work.

## References

1. Deitch EA, Winterton J, Li M, Berg R. The gut as a portal of entry for bacteremia. role of protein malnutrition. *Ann Surg.* 1987;205:681. doi:10.1097/0000658-198706000-00010
2. Huel T, Spicak J. Complications of percutaneous endoscopic gastrostomy. *Best Pract Res Clin Gastroenterol.* 2016;30:769–781. doi:10.1016/j.bpg.2016.10.002
3. Bischoff SC, Austin P, Boeykens K, et al. ESPEN guideline on home enteral nutrition. *Clin Nutr.* 2020;39:5–22. doi:10.1016/j.clnu.2019.04.022
4. Itkin M, DeLegge MH, Fang JC, et al. Multidisciplinary practical guidelines for gastrointestinal access for enteral nutrition and decompression from the society of interventional radiology and American Gastroenterological Association (AGA) Institute, with endorsement by Canadian Interventional Radiological Association (CIRA) and Cardiovascular and Interventional Radiological Society of Europe (CIRSE). *Gastroenterology.* 2011;141:742–765. doi:10.1053/j.gastro.2011.06.001
5. Roveron G, Antonini M, Barbierato M, et al. Clinical practice guidelines for the nursing management of percutaneous endoscopic gastrostomy and jejunostomy (PEG/PEJ) in adult patients: an executive summary. *J Wound Ostomy Cont Nurs.* 2018;45:326–334. doi:10.1097/WON.0000000000000442

6. Gottlieb K, Iber FL, Livak A, Leya J, Mobarhan S. Oral Candida colonizes the stomach and gastrostomy feeding tubes. *J Parenteral Enteral Nutr.* 1994;18:264–267. doi:10.1177/0148607194018003264
7. Arvanitakis M, Gkolfakis P, Despott EJ, et al. Endoscopic management of enteral tubes in adult patients—part 1: definitions and indications. *ESGE Guideline Endoscopy.* 2021;53:81–92.
8. Rosenberger LH, Newhook T, Schirmer B, Sawyer RG. Late accidental dislodgement of a percutaneous endoscopic gastrostomy tube: an underestimated burden on patients and the health care system. *Surg Endosc.* 2011;25(10):3307–3311. doi:10.1007/s00464-011-1709-y
9. Boeykens K, Duysburgh I. Prevention and management of major complications in percutaneous endoscopic gastrostomy. *BMJ Open Gastroenterol.* 2021;8:e000628. doi:10.1136/bmjgast-2021-000628
10. Blumenstein I, Borger D, Loitsch S. A glycerin hydrogel-based wound dressing prevents peristomal infections after Percutaneous Endoscopic Gastrostomy (PEG). *Nutr Clin Pract.* 2012;27(3):422–425. doi:10.1177/0884533612444536
11. Simões D, Miguel SP, Ribeiro MP, Coutinho P, Mendonça AG, Correia IJ. Recent advances on antimicrobial wound dressing: a review. *Eur J Pharm Biopharm Official JArbeitsgemeinschaft Fur Pharmazeutische Verfahrenstechnik E V.* 2018;127:130–141.
12. Rajan A, Wangrattanapranee P, Kessler J, Kidambi TD, Tabibian JH. Gastrostomy tubes: fundamentals, peri-procedural considerations, and best practices. *World J Gastrointest Surg.* 2022;14(4):286–303. doi:10.4240/wjgs.v14.i4.286
13. Alsunaid S, Holden VK, Kohli A, Diaz J, O'Meara LB. Wound care management: tracheostomy and gastrostomy. *J Thorac Dis.* 2021;13(8):5297–5313. doi:10.21037/jtd-2019-ipicu-13
14. Schreml S, Szeimies R, Prantl L, Karrer S, Landthaler M, Babilas P. Oxygen in acute and chronic wound healing. *Br J Dermatol.* 2010;163:257–268. doi:10.1111/j.1365-2133.2010.09804.x
15. Sen CK. The general case for redox control of wound repair. *Wound Repair Regen.* 2003;11:431–438. doi:10.1046/j.1524-475X.2003.11607.x
16. Rodriguez PG, Felix FN, Woodley DT, Shim EK. The role of oxygen in wound healing: a review of the literature. *Dermatologic Surg.* 2008;34(9):1159–1169. doi:10.1111/j.1524-4725.2008.34254.x
17. Li W-P, Su C-H, Wang S-J, et al. CO<sub>2</sub> delivery to accelerate incisional wound healing following single irradiation of near-infrared lamp on the coordinated colloids. *ACS nano.* 2017;11:5826–5835. doi:10.1021/acsnano.7b01442
18. Desmet CM, Pr at V, Gallez B. Nanomedicines and gene therapy for the delivery of growth factors to improve perfusion and oxygenation in wound healing. *Adv Drug Delivery Rev.* 2018;129:262–284. doi:10.1016/j.addr.2018.02.001
19. Cowan L, Stechmiller J, Phillips P, Schultz G. Science of wound healing: translation of bench science into advances for chronic wound care. *chronic wound care—A clinical source book for healthcare professionals.* In: *Communications.* 5th ed. Malvern, PA: HMP LLC; 2012:25–35.
20. Valko M, Leibfritz D, Moncol J, Cronin MT, Mazur M, Telser J. Free radicals and antioxidants in normal physiological functions and human disease. *Int J Biochem Cell Biol.* 2007;39(1):44–84. doi:10.1016/j.biocel.2006.07.001
21. Wu H, Li F, Shao W, Gao J, Ling D. Promoting angiogenesis in oxidative diabetic wound microenvironment using a nanozyme-reinforced self-protecting hydrogel. *ACS Cent Sci.* 2019;5(3):477–485. doi:10.1021/acscentsci.8b00850
22. Mutluoglu M, Cakkalkurt A, Uzun G, Aktas S. Topical oxygen for chronic wounds: a PRO/CON debate. *J Am College Clin Wound Spec.* 2013;5:61–65. doi:10.1016/j.jccw.2014.12.003
23. Zhu J, Jiang G, Hong W, et al. Rapid gelation of oxidized hyaluronic acid and succinyl chitosan for integration with insulin-loaded micelles and epidermal growth factor on diabetic wound healing. *Mater Sci Eng C.* 2020;117:111273. doi:10.1016/j.msec.2020.111273
24. Balazs EA, Laurent TC, Jeanloz RW. Nomenclature of hyaluronic acid. *Biochem J.* 1986;235:903. doi:10.1042/bj2350903
25. Yang R, Liu X, Ren Y, et al. Injectable adaptive self-healing hyaluronic acid/poly ( $\gamma$ -glutamic acid) hydrogel for cutaneous wound healing. *Acta Biomater.* 2021;127:102–115. doi:10.1016/j.actbio.2021.03.057
26. Alonci G, Mocchi R, Sommatis S, et al. Physico-chemical characterization and in vitro biological evaluation of a bionic hydrogel Based on hyaluronic acid and l-lysine for medical applications. *Pharmaceutics.* 2021;13:1194. doi:10.3390/pharmaceutics13081194
27. Reitingner S, Lepperdinger G. Hyaluronan, a ready choice to fuel regeneration: a mini-review. *Gerontology.* 2012;59:71–76. doi:10.1159/000342200
28. Lin L, Xue L, Durairasan S, Haiying C. Cui haiying: preparation of  $\epsilon$ -polylysine/chitosan nanofibers for food packaging against salmonella on chicken. *Food Pack Shelf Life.* 2018;17:134–141. doi:10.1016/j.fpsl.2018.06.013
29. Schmidt S, Madaboosi N, Uhlig K, et al. Control of cell adhesion by mechanical reinforcement of soft polyelectrolyte films with nanoparticles. *Langmuir.* 2012;28:7249–7257. doi:10.1021/la300635z
30. Zhang Z, Zeng X, Brennan CS, Ma H, Aadil RM. Preparation and characterisation of novelty food preservatives by Maillard reaction between  $\epsilon$ -polylysine and reducing sugars. *Int J of Food Sci Tech.* 2019;54:1824–1835. doi:10.1111/ijfs.14083
31. Shahriari-Khalaji M, Li G, Liu L, et al. A poly-l-lysine-bonded TEMPO-oxidized bacterial nanocellulose-based antibacterial dressing for infected wound treatment. *Carbohydr Polym.* 2022;287:119266. doi:10.1016/j.carbpol.2022.119266
32. Varaprasad K, Jayaramudu T, Kanikireddy V, Toro C, Sadiku ER. Alginate-based composite materials for wound dressing application: a mini review. *Carbohydr Polym.* 2020;236:116025. doi:10.1016/j.carbpol.2020.116025
33. Sood A, Granick MS, Tomaselli NL. Wound dressings and comparative effectiveness data. *Adv Wound Care.* 2014;3:511–529. doi:10.1089/wound.2012.0401
34. Wang L, Shelton R, Cooper P, Lawson M, Triffitt J, Barralet J. Evaluation of sodium alginate for bone marrow cell tissue engineering. *Biomaterials.* 2003;24:3475–3481. doi:10.1016/S0142-9612(03)00167-4
35. Yadav P, Yadav H, Shah VG, Shah G, Dhaka G. Biomedical biopolymers, their origin and evolution in biomedical sciences: a systematic review. *J Clin Diagn Res.* 2015;9:ZE21. doi:10.7860/JCDR/2015/13907.6565
36. Kamoun EA, Kenawy E-RS, Chen X. A review on polymeric hydrogel membranes for wound dressing applications: PVA-based hydrogel dressings. *J Adv Res.* 2017;8:217–233. doi:10.1016/j.jare.2017.01.005
37. Guo J, Wei C, Wang X, Hou Y, Guo W. An in situ mechanical adjustable double crosslinking hyaluronic acid/poly-lysine hydrogel matrix: fabrication, characterization and cell morphology. *Int J Biol Macromol.* 2021;180:234–241. doi:10.1016/j.ijbiomac.2021.03.071
38. Liu S, Liu X, Ren Y, et al. Mussel-inspired dual-cross-linking hyaluronic acid/ $\epsilon$ -polylysine hydrogel with self-healing and antibacterial properties for wound healing. *ACS Appl Mater Interfaces.* 2020;12:27876–27888. doi:10.1021/acsmi.0c00782
39. Benito-Martinez S, P erez-K ohler B, Rodriguez M, Izco JM, Recalde JI, Pascual G. Wound healing modulation through the local application of powder collagen-derived treatments in an excisional cutaneous murine model. *Biomedicines.* 2022;10(5):960. doi:10.3390/biomedicines10050960

40. Chen Q, Feng L, Liu J, et al. Intelligent albumin–MnO<sub>2</sub> nanoparticles as pH-/H<sub>2</sub>O<sub>2</sub>-responsive dissociable nanocarriers to modulate tumor hypoxia for effective combination therapy. *Adv Mater.* 2016;28:7129–7136. doi:10.1002/adma.201601902
41. Asayama S, Nogawa M, Takei Y, Akaike T, Maruyama A. Synthesis of novel polyampholyte comb-type copolymers consisting of a poly (L-lysine) backbone and hyaluronic acid side chains for a DNA carrier. *Bioconjugate Chem.* 1998;9:476–481. doi:10.1021/bc970213m
42. Wang W, Ummartyotin S, Narain R. Advances and challenges on hydrogels for wound dressing. *Curr Opin Biomed Eng.* 2023;26:100443. doi:10.1016/j.cobme.2022.100443
43. Rao KM, Suneetha M, Zo S, Duck KH, Han SS. One-pot synthesis of ZnO nanobelt-like structures in hyaluronan hydrogels for wound dressing applications. *Carbohydr Polym.* 2019;223:115124. doi:10.1016/j.carbpol.2019.115124
44. Pangiantuk A, Kaokaen P, Kunhorm P, Chaicharoenaudomrung N, Noisa P. 3D culture of alginate-hyaluronic acid hydrogel supports the stemness of human mesenchymal stem cells. *Sci Rep.* 2024;14(1):4436. doi:10.1038/s41598-024-54912-1
45. Rowley JA, Madlambayan G, Mooney DJ. Alginate hydrogels as synthetic extracellular matrix materials. *Biomaterials.* 1999;20(1):45–53. doi:10.1016/S0142-9612(98)00107-0
46. Zheng M, Pan M, Zhang W, et al. Poly ( $\alpha$ -l-lysine)-based nanomaterials for versatile biomedical applications: current advances and perspectives. *Bioact Mater.* 2021;6:1878–1909. doi:10.1016/j.bioactmat.2020.12.001
47. Yang R, Huang J, Zhang W, et al. Mechanoadaptive injectable hydrogel based on poly ( $\gamma$ -glutamic acid) and hyaluronic acid regulates fibroblast migration for wound healing. *Carbohydr Polym.* 2021;273:118607. doi:10.1016/j.carbpol.2021.118607
48. Brewer AR, Smyrk TC, Bailey RT Jr, Bonavina L, Eypasch EP, Demeester TR. Drug-induced esophageal injury. Histopathological study in a rabbit model. *Dig Dis Sci.* 1990;35(10):1205–1210. doi:10.1007/BF01536408
49. Che C, Liu L, Wang X, et al. Surface-adaptive and on-demand antibacterial sponge for synergistic rapid hemostasis and wound disinfection. *ACS Biomater Sci Eng.* 2020;6(3):1776–1786. doi:10.1021/acsbiomaterials.0c00069
50. Li Q, Zheng L, Guo Z, Tang T, Zhu B. Alginate degrading enzymes: an updated comprehensive review of the structure, catalytic mechanism, modification method and applications of alginate lyases. *Crit Rev Biotechnol.* 2021;41(6):953–968. doi:10.1080/07388551.2021.1898330

International Journal of Nanomedicine

Publish your work in this journal

The International Journal of Nanomedicine is an international, peer-reviewed journal focusing on the application of nanotechnology in diagnostics, therapeutics, and drug delivery systems throughout the biomedical field. This journal is indexed on PubMed Central, MedLine, CAS, SciSearch®, Current Contents®/Clinical Medicine, Journal Citation Reports/Science Edition, EMBase, Scopus and the Elsevier Bibliographic databases. The manuscript management system is completely online and includes a very quick and fair peer-review system, which is all easy to use. Visit <http://www.dovepress.com/testimonials.php> to read real quotes from published authors.

Submit your manuscript here: <https://www.dovepress.com/international-journal-of-nanomedicine-journal>

**Dovepress**  
Taylor & Francis Group